AD-A046 084 GEORGIA INST OF TECH ATLANTA F/G 20/4
A NUMERICAL STUDY OF VISCOUS FLOWS AROUND AIRFOILS.(U)
SEP 77 J C WU, S SAMPATH, L N SANKAR N00014-75-C-0249
UNCLASSIFIED NL

| OF |
AD
A046084

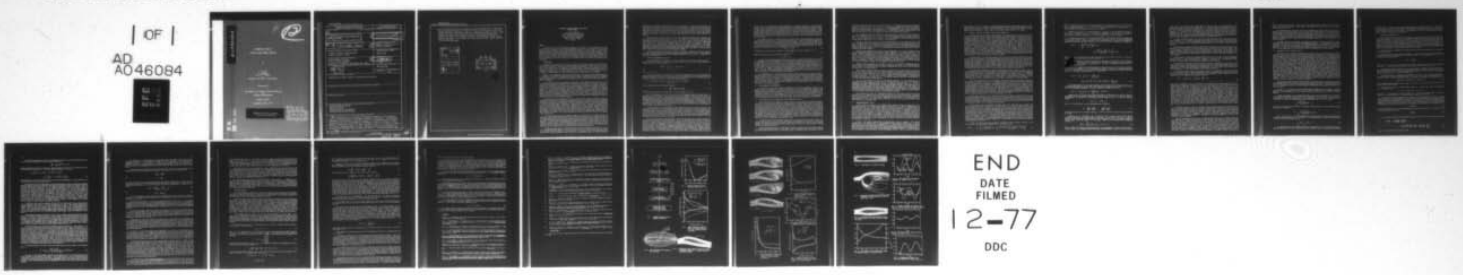

END
DATE
FILMED
12-77
DDC

A NUMERICAL STUDY OF VISCOUS FLOWS AROUND AIRFOILS

by

J. C. Wu
S. Sampath
and N. L. Sankar
of
Georgia Institute of Technology

Presented at

The AGARD Fluid Dynamics Panel Symposium
on
Unsteady Aerodynamics

Ottawa, Canada

September 26-28, 1977

Unclassified

SECURITY CLASSIFICATION OF THIS PAGE (When Data Entered)

REPORT DOCUMENTATION PAGE	READ INSTRUCTIONS BEFORE COMPLETING FORM
1. REPORT NUMBER (6)	2. GOVT ACCESSION NO. / 3. RECIPIENT'S CATALOG NUMBER
4. TITLE (and Subtitle) A NUMERICAL STUDY OF VISCOUS FLOWS AROUND AIRFOILS,	(9) 5. TYPE OF REPORT & PERIOD COVERED Interim Technical Report, / 6. PERFORMING ORG. REPORT NUMBER
7. AUTHOR(s) (10) J. C. Wu, S. Sampath, and L. N. Sankar	(15) 8. CONTRACT OR GRANT NUMBER(s) N00014-75-C-0249
9. PERFORMING ORGANIZATION NAME AND ADDRESS Georgia Institute of Technology Atlanta, Georgia 30332	10. PROGRAM ELEMENT, PROJECT, TASK AREA & WORK UNIT NUMBERS NR-061-226
11. CONTROLLING OFFICE NAME AND ADDRESS Fluid Dynamics Program Office of Naval Research Department of the Navy Arlington, VA 22217	(11) 12. REPORT DATE September 1977 / 13. NUMBER OF PAGES 18
14. MONITORING AGENCY NAME & ADDRESS (if different from Controlling Office) (12) 21p.	15. SECURITY CLASS. (of this report) Unclassified / 15a. DECLASSIFICATION/DOWNGRADING SCHEDULE N/A

16. DISTRIBUTION STATEMENT (of this Report)

Approved for public release, distribution unlimited.

17. DISTRIBUTION STATEMENT (of the abstract entered in Block 20, if different from Report)

18. SUPPLEMENTARY NOTES

19. KEY WORDS (Continue on reverse side if necessary and identify by block number)

Navier-Stokes Equations
Separated Flows
Computational Fluid Dynamics
Integro-Differential Method

20. ABSTRACT (Continue on reverse side if necessary and identify by block number)

The application of an integro-differential approach in the numerical study of unsteady viscous flows about airfoils is described. Two different procedures are presented. A procedure based on a stream function-vorticity formulation and on a transformation technique is used in a study of a flow about an impulsively started 9% thick Joukowski airfoil at an angle of attack of 15° and a Reynolds number of 1000. Numerical results are presented and compared with available finite-difference results. A second procedure based

DD FORM 1 JAN 73 1473 EDITION OF 1 NOV 65 IS OBSOLETE

Unclassified

SECURITY CLASSIFICATION OF THIS PAGE (When Data Entered)

153 800

on a velocity-vorticity formulation and on a hybrid finite difference-finite element technique is used in a study of a flow about an oscillating 12% thick Joukowski airfoil at a Reynolds number of 1000. With either procedure, the unique ability of the integro-differential approach to confine the solution field to the vortical region of the flow is utilized. It is shown that this ability offers great computational advantages.

A NUMERICAL STUDY OF UNSTEADY VISCOUS FLOWS AROUND AIRFOILS

J. C. Wu, Professor
S. Sampath, Research Assistant
and N. L. Sankar, Research Assistant
School of Aerospace Engineering
Georgia Institute of Technology
Atlanta, Georgia 30332
U.S.A.

SUMMARY

The application of an integro-differential approach in the numerical study of unsteady viscous flows about airfoils is described. Two different procedures are presented. A procedure based on a stream function-vorticity formulation and on a transformation technique is used in a study of a flow about an impulsively started 9% thick Joukowski airfoil at an angle of attack of 15^{o} and a Reynolds number of 1000. Numerical results are presented and compared with available finite-difference results. A second procedure based on a velocity-vorticity formulation and on a hybrid finite difference-finite element technique is used in a study of a flow about an oscillating 12% thick Joukowski airfoil at a Reynolds number of 1000. With either procedure, the unique ability of the integro-differential approach to confine the solution field to the vortical region of the flow is utilized. It is shown that this ability offers great computational advantages.

1. INTRODUCTION

During the past two decades, there has been a gradual but persistent increase in the willingness of aerodynamicists to accept the computer as a valuable, perhaps indispensable, tool in the prediction of fluid flows. This willingness is a consequence of the impressive progress made in recent years in the routine numerical solutions of differential equations describing many types of potential and boundary layer flows. For general viscous flows, i.e., flows past finite solid bodies and involving appreciable regions of separation, a capability for the routine computation of the flows has yet to be established, and the willingness to accept computer solutions has spurred extensive research efforts in this regard.

Because of its fundamental nature and practical importance, the general viscous flow problem has been a focal point of fluid dynamic research for more than a century. The mathematical difficulties attendant to the analytical solution of the equations describing the general viscous flow are known to be formidable. Numerical methods offer at the present the only prospect of accurate quantitative solutions under reasonably general circumstances.

Until relatively recently, computational aerodynamicists have emphasized the application of the finite-difference approach to the general viscous flow problem. This emphasis is an outgrowth of the success enjoyed by the finite-difference methods in the solution of various boundary layer problems. Although the boundary layer equations are simpler than the Navier-Stokes equations describing the general viscous flow, the two types of equations are both non-linear partial difference equations. Furthermore, the momentum equation for the time-dependent general viscous flow is parabolic, as is the boundary layer momentum equation. It had been hoped, therefore, that the finite-difference approach would lead to a routine computational capability for the time-dependent general viscous flow, with steady flow solutions, when they exist, considered as asymptotic limiting solutions at large time levels. In reality, however, the application of the finite-difference approach to the general viscous flow problem has fallen far short of earlier expectations. Most of the general viscous flows of practical importance in aerodynamics today remain beyond the scope of the finite-difference approach.

Several years ago, the first author of this article identified several major obstacles that caused the disparity of successes of the finite-difference approach as applied to the boundary layer and to the general incompressible viscous flows. Subsequently, a program of research was initiated with the goal of developing new approaches transcending the limitations of the finite-difference approach. This research program has now reached a reasonable stage of completeness. Progress made to date in applying a new approach to the study of unsteady incompressible laminar flows is summarized in this paper. Selected numerical results are presented for flows past airfoils to illustrate the application of this new approach. Additional numerical results as well as detailed descriptions of the specific numerical procedures are presented in doctoral dissertations of the second author (Ref. 1) and of the third author, the latter still being prepared. A major emphasis of the present article is to bring into focus the authors' understanding, acquired during the past few years of research, of the interplay between the numerical and physical aspects of the general viscous flow problem.

The distinguishing feature of the present approach is the formulation of the general viscous flow problem as a set of integro-differential equations. This feature represents a major departure from finite-difference methods based on the formulation of the problem as differential equations. Various attributes of the integro-differential approach have been studied and described in earlier articles (Refs. 1 to 11). In particular, it has been conclusively demonstrated by analyses and numerical illustrations that the approach possesses a unique ability to confine the solution field to the vortical region of the flow. For most problems of practical interest, the flow Reynolds number is high and the vortical region represents only a small fraction of the total flowfield. The ability to confine the solution field to the vortical region therefore offers the possibility of a drastically improved computational efficiency.

Although the present paper is concerned only with unsteady incompressible laminar flows, the utility of the integro-differential approach is not restricted to such flows. In a recent article (Ref. 3), the use of the integro-differential approach in conjunction with a two-equation turbulence model was demonstrated. Turbulent flow results obtained were found to agree well with experimental data. An integro-differential

formulation was presented for compressible flows three years ago (Ref. 4). Because of the limited resources available, however, efforts of the present authors in implementing the integro-differential approach have been limited to incompressible flow problems. It has also been found that the general viscous flow problem may be formulated as a set of integral representations (Ref. 5) of field variables. The solution procedures developed for the integro-differential approach are directly applicable to methods based on the integral-representation approach. In particular, for steady flows, a method based on the integral representation approach has been established (Ref. 6) and a general computer code for internal flow problems is being prepared.

Recent literature contains several articles by other researchers describing results obtained using the integro-differential approach (Refs. 12 to 15). The relatively large amounts of computing needs associated with these efforts as well as with our earlier work (Ref. 7) led to the opinion that, even though the integro-differential approach permits the solution field to be confined to the vortical region of the flow, the approach is computationally inefficient (Ref. 16). This impression is misleading. The present authors have, in the past few years, progressed through several stages of development of the integro-differential approach; each stage has led to a substantial reduction in computing need. The present computing need is about 1/20 of that reported in Ref. 7 and for two-dimensional problems is about 1/5 of that required by the more efficient finite-difference methods available today. The reduction in needed computer time is expected to be much greater for three-dimensional problems.

Two different numerical procedures are outlined in this paper. A procedure utilizing a transformation technique is used in a study of a flow about an impulsively started 9% thick airfoil. A second procedure utilizing a hybrid finite difference-finite element technique is used in a study of flows about an oscillating 12% thick airfoil.

2. KINETICS AND KINEMATICS OF THE FLOW

The time-dependent Navier-Stokes and continuity equations for a fluid with constant density ρ, constant kinematic viscosity ν, and subject to negligible body forces are well-known and are expressible in terms of the velocity $\vec{v}$ and pressure p as:

$$\frac{\partial \vec{v}}{\partial t} + (\vec{v} \cdot \vec{\nabla})\vec{v} = -\frac{1}{\rho}\vec{\nabla}p + \nu\nabla^2\vec{v} \tag{1}$$

and

$$\vec{\nabla} \cdot \vec{v} = 0 \tag{2}$$

where t is the time.

Equations (1) and (2) are in principle sufficient for the determination of $\vec{v}$ and p, provided that adequate initial and boundary conditions are known. The boundary conditions occuring most frequently are the "no-slip" condition at the surface of solid bodies over which the fluid passes. For problems involving an infinite fluid domain, $\vec{v}$ and p at infinity must also be specified.

It is convenient to introduce the vorticity vector $\vec{\omega}$ defined by

$$\vec{\nabla} \times \vec{v} = \vec{\omega} \tag{3}$$

and to consider the "vorticity transport" equation

$$\frac{\partial \vec{\omega}}{\partial t} = \vec{\nabla} \times (\vec{v} \times \vec{\omega}) + \nu\nabla^2\vec{\omega} \tag{4}$$

obtained by taking the curl of both sides of Eq. (1) and using Eqs. (2) and (3).

The set of equations (2) to (4), with $\vec{v}$ and $\vec{\omega}$ as dependent variables, replaces the set of equations (1) and (2) in which $\vec{v}$ and p are dependent variables. There are several reasons for using $\vec{\omega}$ in the formulation of the problem. A principal reason is that the formulation in terms of $\vec{\omega}$ allows clear and separate delineation of the kinetic and kinematic aspects of the problem. As a consequence of this clear delineation several important characteristics of the general viscous flow problem, not obvious in the p and $\vec{v}$ formulation, become manifest. Major obstacles to the finite-difference solution of the general viscous flow problem are then traceable to physical processes involved in the development of the flow patterns. The identification of the physical origin of these obstacles is of course a prerequisite for the establishment of solution methods that overcome these obstacles.

The kinetic aspect of the problem deals with the change of the vorticity field $\vec{\omega}$ with time. This aspect is described by Eq. (4). For an inviscid fluid, the last term in Eq. (4) vanishes and the vorticity is convected with the fluid in the sense that the vorticity flux $\vec{\omega} \cdot \vec{n}\,ds$, where $\vec{n}$ is a unit normal vector of the surface element ds, associated with each material element ds moving with the fluid remains a constant for all times. This well-known theorem of Helmholtz is modified in the case of a real fluid by the process of vorticity diffusion. According to Eq. (4), changes in the flux of vorticity across a surface element that is moving with the fluid and is in the interior of the fluid domain takes place only by diffusion. Vorticity flux cannot be created in the interior of a fluid.

If the fluid is in contact with solid bodies in motion, the no-slip condition provides a mechanism for the generation of vorticity at the solid surfaces. In the case where the fluid is initially at rest and occupies an infinite domain bounded internally by surfaces of solid bodies also initially at rest, the vorticity is obviously zero everywhere initially. Subsequent motion of the solid bodies sets up corresponding motion of the fluid. Immediately after the onset of the motion, since the vorticity flux in the interior of the fluid domain can change only as a consequence of diffusion, the vorticity is everywhere zero except at the solid surfaces. That is, the flow immediately after the onset of the motion has a non-zero tangential velocity relative to the solid bodies at the solid boundaries. The discontinuity in tangential velocity represents a sheet of concentrated vorticity at the solid boundaries. At subsequent time levels, this concentrated vorticity at the solid boundaries spreads into the interior of the fluid domain by diffusion

and, once there, is transported away from the boundaries by both convection and diffusion. At the same time, vorticity is continually generated on the solid boundaries. The general flow pattern therefore includes vortical regions surrounding the solid bodies and vortical wake regions trailing the solid bodies. Outside of these vortical regions, the flow is essentially free of vorticity and is therefore potential. If the Reynolds number of the flow is not small, then the vorticity spreads by diffusion only a short distance from the solid surface before being carried away with the fluid. Thus there exists a large region of the fluid, ahead and to the side of the solid bodies, which is free of vorticity. In fact, at any finite time level after the onset of the motion, the vortical regions are finite in extent while the potential flow region is infinite in extent.

The kinematic aspect of the problem relates the velocity field at any given instant of time to the vorticity field at that instant. This aspect is described by Eqs. (2) and (3) together with appropriate velocity boundary conditions on the solid surfaces and at infinity. If the velocity field is known at any given instant of time, the corresponding vorticity field is immediately obtainable by differention, using Eq. (3). If the vorticity field is known, the velocity field is obtainable by integrating Eq. (3), subject to the solenoidal condition, Eq. (2). One method of evaluating $\vec{v}$ is to take the curl of Eq. (3) and, by using Eq. (2), obtain a vector Poisson's equation for $\vec{v}$ in the form

$$\nabla^2 \vec{v} = -\vec{\nabla} \times \vec{\omega} \tag{5}$$

Alternatively, Eq. (2) implies the existence of a vector potential $\vec{\Psi}$ which is related to $\vec{v}$ by

$$\vec{v} = \vec{\nabla} \times \vec{\Psi} \tag{6}$$

Equation (3) and (6) gives a vector Poisson's equation:

$$\nabla \times \nabla \times \vec{\Psi} = \vec{\omega} \tag{7}$$

A general solution procedure based on the kinetic-kinematic formulation which enables the pattern of flow development to be followed computationally is as follows. With known spatial distributions of $\vec{v}$ and $\vec{\omega}$ at a given time level, the kinetic aspect, i.e., Eq. (4) together with appropriate boundary conditions on ω, is treated numerically and a new distribution of vorticity at a subsequent time level is established. The kinematic aspect, i.e., Eqs. (2) and (3), or Eq. (7), together with appropriate boundary conditions for $\vec{v}$, or $\vec{\Psi}$, is then treated and a new velocity distribution corresponding to the new vorticity distribution at the new time level is obtained. This completes a computational loop to advance the solution from an old time level to a new one. Repeated applications of this computational loop yields a transient solution. In the limit of large time, if the velocity boundary conditions are independent of time, then either a steady state solution or a periodic vortex shedding solution is obtainable.

The implementation of the above outlined solution procedure consists of a number of component problems as shown in Figure 1. The literature contains a variety of numerical methods that differ from one another in the specific techniques for treating the component problems. The general framework for these numerical methods, however, are identical. If the "primitive" variable p is used in place of the "derived" variable ω, or if $\vec{\Psi}$ is used in place of $\vec{v}$, the component problems are then concerned with the computation of these different variables. The spirit of the general solution-procedure framework, however, remains the same. The major difficulties encountered by researchers can be conveniently reviewed by a critical examination of the component problems.

3. MAJOR OBSTACLES AND ALTERNATIVES

In this section, several major obstacles experienced in previous finite-difference solutions of the general viscous flow problem are reviewed. As stated earlier, the finite-difference approach enjoys remarkable success in the prediction of boundary layer flows. The present obstacles are traceable to the important differences between the boundary layer flow and the general viscous flow in flow patterns and in the physical processes of flow development. It is worthy of note that except the establishment of the initial solution, each of the component problems for the general viscous flow, as shown in Fig. 1, present difficulties that are absent in the boundary layer flow. These difficulties dictate the development of innovative approaches for the general viscous flow problem. Several such approaches are described here.

3.1. Grid System--Coordinate-Transformation and Finite-Element Methods

As discussed earlier, the flowfield in general consists of vortical regions surrounded by a potential flow region. For high Reynolds number flows, if no appreciable flow reversal occurs near the solid bodies, the vorticity spreads to the sides of the solid bodies mainly by diffusion. Since the diffusive process is relatively slow at high Reynolds numbers, the vortical regions near the solid bodies are thin and the boundary layer simplifications are justifiable there. The vortical wakes derive their vorticity from the thin boundary layers and are therefore also thin. The success of the boundary layer theory is attributable to the fact that the effects of these vortical layers on the potential flow may be treated as a relatively small perturbation to the potential flow past the solid bodies in the absence of the vortical layers. This fact permits the potential region to be studied separately from the vortical regions. In particular, it becomes possible to establish the flow velocity immediately adjacent to the boundary layer through potential flow analyses, employing iterative or matching procedures if needed to properly account for the effects of the vortical layers. Consequently, it is possible to confine the solution field of the boundary layer equation to the thin vortical layers near the solid bodies.

In general viscous flows, appreciable regions of flow reversal occur near the solid bodies. The vorticity now spreads to the sides of the solid bodies by both diffusion and convection. The vortical regions are not thin and their presence "strongly" influences the potential flow. With the finite-difference approach, the solution field must include the potential region as well as the vortical regions. Matching procedures are not easily applicable.

For attached boundary layers, it is permissible to employ an orthogonal coordinate system with one of the coordinate axes coinciding with the solid surface. Such a coordinate system is curvilinear. However, since the solution field is restricted to the thin region of the boundary layer, the scale factor of the

curvilinear system changes negligibly across the solution field. The differential equations describing the flow, when expressed in terms of the curvilinear coordinates, are formally identical with the equations expressed in the Cartesian coordinates, the curvature terms being negligibly small within the context of boundary-layer approximations. As a consequence, it is straightforward to use a finite-difference grid system with the airfoil surface represented by a grid line. Such a grid system is "boundary-fitted" in the sense that data points on the solid boundaries are permitted to coincide with grid points.

For the general viscous flow problem, the solution field is not thin and the scale factor in a curvilinear coordinate system fitted to the solid boundaries can change substantially across the solution field. The differential equations describing the flow, when expressed in the curvilinear coordinates, contain curvature terms that are not negligible. The use of a boundary-fitted finite-difference grid is considerably more complex than it is in the case of an attached flow.

Much of the earlier works using the finite-difference approach to treat the general viscous flow problem attempted to avoid the complexity introduced by the use of curvilinear coordinate system. In these works, the differential equations are expressed in Cartesian Coordinates and a rectangular grid system in the physical plane is used. Such a system is not boundary-fitted. That is, grid points representing the boundary in general do not coincide with the solid boundaries, and interpolation procedures are needed to accommodate the boundary geometry.

Various authors treating different types of flow problems (Refs. 17 to 21) are in agreement that the proper handling of the boundary conditions are of dominant importance in the numerical solution of flow problems. Existing evidence points to the use of grid systems that are not body-fitted as one of the culprits for the very limited capability of earlier methods in treating the general viscous flow problem. As is well-known, the Navier-Stokes equations describing the general viscous flow are common to an astonishingly rich variety of flow phenomena drastically differing from one another not only quantitatively but also in character. The drastic differences are results of differences in the geometries and the imposed conditions at the flow boundaries. Clearly, accurate representation of the flow boundaries and of the boundary conditions are of paramount importance in the prediction of general viscous flows.

Boundary-fitted grid systems are obtainable by the use of coordinate transformation methods. Alternatively, the finite-element methods (Ref. 18) accomplish the same purpose. With either approach, the relative simplicity of the Cartesian finite-difference representation are bartered for a better numerical representation of the boundary geometry.

Until recently, successful numerical solutions of the general viscous flow problem have been obtained only for those boundary geometries for which convenient analytical transformation formulas are available. In particular, conformal transformations which permit straight forward calculation of the scale factor for the curvilinear coordinate system and of the curvature terms in the differential equations have been utilised by several researchers. In recent years, numerical methods for the establishment of boundary-fitted coordinate systems have been developed (Ref. 17). The numerical transformations need not be conformal and is not restrictive regarding the boundary geometry.

The basic finite-element methods involves the following components: (a) the reformulation of the differential equations as integral relations, (b) the division of the solution field, i.e., the region of integration, into small subregions, called elements, of arbitrary sizes and shapes, (c) the use of interpolation functions, usually polynomials, to express the dependent variables in each element in terms of their values at selected data points, called nodes, associated with the element, and (d) the evaluation of the integrals over each element, yielding a set of algebraic equations containing the nodal values of the dependent variables as unknowns. Since the elements are of arbitrary sizes and shapes, it is straightforward to devise a boundary-fitted system of elements. The resulting set of algebraic equations, however, possesses coefficient matrices more complex than those of finite-difference equations.

In the present work, both the transformation method and the finite-element method are utilized in conjunction with the integro-differential approach in studies of viscous flows about airfoils. The studies demonstrated that both methods are effective in removing the difficulty of accurate numerical representation of the solid boundaries. The added algebraic complexity of either method is not excessive for two-dimensional flows. There exist, however, several other difficulties that are not removed by either method. These difficulties are described below.

3.2. Vorticity Solution - Kinetics

A major source of difficulty in the kinetic part of general viscous flow computation is the simultaneous occurrence of the diffusive and convective processes in the flow. These two processes proceed at drastically different rates at high Reynolds numbers. The length and time scales of these processes are vastly different. This fact leads to vastly different, often overly stringent, requirements on the time interval and grid spacing because of accuracy and stability considerations. In comparison to problems in which either the diffusive process or the convective process is alone important, the kinetic aspect of the general viscous flow is immensely more complex. For boundary layer flows in two-dimensions, the diffusive process is of negligible importance in comparison to the convective process along the direction parallel to the body surface. In the direction perpendicular to the body surface, the convective and diffusive processes are of comparable importance and the length scales of the two processes are not vastly different. Consequently, the boundary layer momentum equations do not contain the above described difficulty associated with the general viscous flow.

In Ref. 5, an integral representation for the vorticity vector is presented. This integral representation is completely equivalent to the differential vorticity transport equation (4). A solution procedure based on this representation is suggested in Ref. 5. This procedure has been calibrated recently using simple problems with known analytical solutions. A noteworthy feature of this procedure is that the kinetic processes of diffusion and convection are represented by separate integrals and the contributions of these two processes to the time variation of vorticity can be evaluated separately in a convenient manner. This new procedure is being developed for complex time-dependent problems. The work reported in the present

paper, however, are based on extensions of existing finite-difference and finite-element methods. For the impulsively started airfoil, a method of flowfield segmentation is developed and used in conjunction with a modified strongly implicit procedure. For the oscillating airfoil, a hybrid finite difference-finite element method is established. These methods will be outlined in later sections of this paper.

3.3. Kinematics - Integral Representation and Flowfield Segmentation

It is well known that the computer time requirement for the finite-difference solution of a general viscous flow problem in general increases rapidly with the flow Reynolds number. The basic cause of this difficulty is that the kinematic aspect of the general viscous flow problem is described by elliptic differential equations, e.g. Eq. (5) or Eq. (7). The finite-difference solution of $\vec{v}$ at any given point in the flowfield depends on the value of $\vec{v}$ at the neighboring points. It is therefore not possible to evaluate the value of $\vec{v}$ explicitly, point by point, using a finite-difference method. The solution field, in fact, should be infinite so as to satisfy the freestream condition at infinity. For numerical solution, the infinite solution field needs to be represented by a finite number of grid points. Substantial inaccuracy can result if one truncates the solution field and specifies freestream velocity condition, or some other condition, on some outer boundaries at finite distances from the solid boundary (Reference 8). In many previous works, this outer boundary is placed at a distance of ten chord lengths or more from the solid boundary in hope that the inaccuracy resulting from the replacement of an infinite region by a finite one is then unimportant. Such practices may lead to fundamental difficulties and must be handled with great caution. For example, it can be shown that if the steady state equations are to be treated and the freestream velocity boundary condition is applied at a closed outer boundary at finite distances from the airfoil, then no solution for an airfoil with non-zero lift force is possible.

As discussed earlier, for high Reynolds number flows, the vortical regions surrounding and trailing the solids are relatively small. The effects of viscosity are important only in this region. The gradients of field variables are large and the corresponding length scale for this region is small, particularly in the boundary layer. Consequently, in order to have sufficient solution resolution in this region, the grid lines must be very finely spaced. If this fine spacing is continued into the potential region of the flow, which has been made finite but is still large, a gigantic number of grid points invariably enter the computation procedure. This implies that an excessive amount ofcomputer time is needed to solve the equations. With increasing Reynolds number, the length scale in the vortical region decreases. The number of grid points, and hence also the needed computer time, therefore increases with increasing Reynolds number.

The coordinate transformation and finite-element methods provide a degree of relief from the excessive computing needs at high Reynolds numbers. For example, Ref. 17 describes a method which maps the fluid region into the interior of a rectangle. A uniformly spaced grid system is used in the transformed plane to numerically solve the transformed differential equations. In the physical plane, the corresponding spacing between grid lines increases as the distance from the solid boundaries increases. With the "expanding" grid system in the physical plane, it is possible to substantially reduce the number of grid points entering the solution procedure and to make this number less sensitive to the Reynolds number.

With a finite-element method, since the elements can be of arbitrary sizes and shapes, an expanding grid system is not difficult to devise. To researchers accustomed to the finite-difference approach, the finite-element procedure for setting up a set of algebraic equations may appear to be circuitous. It should be noted, however, that the coordinate transfomration approach, usually considered an improved finite-difference procedure, also would appear to be circuitous to those accustomed to the use of uniformly spaced finite-difference grid in the physical plane. The added complications of coordinate transformation, or of the finite-element approach, however, are amply justified by their ability to accurately represent the boundary geometry, as discussed in Section 3.1. The ability to have an expanding grid system is an additional important property of these approaches. However, these approaches by themselves do not permit an explicit, point by point, evaluation of the velocity values, and therefore the solution field needs to include the potential region as well as the vortical regions of the flow.

As discussed in Section 3.1, in treating the attached flow problem, the solution field for the boundary layer equations can be confined to the thin vortical layers near the solid bodies. There is no need to concurrently solve the potential and the vortical flow problems. Rather, the two problems are solved individually and matched. With attached flows, therefore, the difficulty of simultaneously accommodating the potential and vortical regions is absent. This fact is a major reason contributing to the success of the finite-difference approach in solving boundary layer problems.

For the general viscous flow problem, the kinetic aspect of the computation can be confined to the vortical regions of the flow. From Eq. (4), it is obvious that if the vorticity and velocity fields in the vortical regions are known at any given time level, then the time rate of change of vorticity at that time level is determinate. There is no need to go beyond the vortical regions and their immediate neighborhood to establish a new vorticity distribution at the subsequent time level. Consequently, if the kinematic aspect of the computation can also be confined to the vortical region, then the solution field need not extend into the potential flow region and the difficulty of simultaneously accommodating the potential and the vortical regions is removed. In Ref. 2, it is shown that the confinement of the kinematic aspect of the computation to the vortical region is possible if the differential equations describing the kinematics of the general viscous flow problem is recast into an integral representation of the velocity vector (or of the vector potential). In this research, the integral representation for the kinematics of the problem is used together with the differential vorticity transport equation (4). The formulation of the overall problem is named the integro-differential formulation.

In Ref. 2, it is shown that Eqs. (2) and (3), together with velocity boundary conditions, can be recast into the following integral representation for the velocity vector:

$$\vec{v}(\vec{r},\, t) = -\frac{1}{A}\left[\int_R \frac{\vec{\omega}_o \times (\vec{r}_o - \vec{r})}{|\vec{r}_o - \vec{r}|^d}\, dR_o - \oint_B \frac{(\vec{v}_o \cdot \vec{n}_o)(\vec{r}_o - \vec{r}) - (\vec{v}_o \times \vec{n}_o) \times (\vec{r}_o - \vec{r})}{|\vec{r}_o - \vec{r}|^d}\, dB_o\right] \qquad (8)$$

where $\vec{r}$ is the position vector, $\vec{\omega}$ is the vorticity vector, R is any region occupied by the fluid or the solid, B is the boundary of R, and $\vec{n}$ is the unit normal vector directed outward from R, A = 4π and d = 3 in three-dimensional problems and A = 2π and d = 2 in two-dimensional problems. The subscripts "o" in dR_o and dB_o indicate that the integrations are in the $\vec{r}_o$ space.

Equation (8) is valid for all position vectors in R and on B and is completely equivalent to Eqs. (2) and (3) together with the velocity condition on the boundary B. The use of Eq. (8), in place of Eqs. (2) and (3), permits the explicit, point by point, computation of the velocity distribution in R, provided that the vorticity distribution in R and the velocity condition on B are known.

The second integral in Eq. (8) represents the contribution of the velocity boundary condition to the velocity field within the boundary. For the problem of an external flow past a solid body undergoing translation and rotation, it has been shown (Ref. 8) that this contribution can be expressed in terms of the instantaneous rectilinear and angular velocities, $-\vec{v}_\infty$ and $\vec{\Omega}$, of the solid. Equation (8) then reduces to

$$\vec{v}(\vec{r},\,t) = -\frac{1}{A}\left[\int_{R_f}\frac{\vec{\omega}(\vec{r}_o,\,t)\times(\vec{r}_o-\vec{r})}{|\vec{r}_o-\vec{r}|^d}\,dR_o + 2\int_{R_s}\frac{\vec{\Omega}(\vec{r}_o,\,t)\times(\vec{r}_o-\vec{r})}{|\vec{r}_o-\vec{r}|^d}\,dR_o\right] + \vec{v}_\infty(t) \tag{9}$$

where R_f and R_s are respectively the regions occupied by the fluid and the solid body. The coordinate system translates with the solid but does not rotate with it.

The vortical regions at any finite time level after the onset of the motion are of finite extent and are within finite distances from the solid boundaries. The region of integration is therefore finite. Furthermore, as r goes to infinity, the integrands in Eq. (9) vanish. The freestream boundary condition is satisfied at infinity.

Equation (7), together with appropriate boundary conditions, can be recast into an integral representation for the vector potential $\vec{\Psi}$. For two-dimensional flows, $\vec{\Psi}$ has only one non-vanishing component in the direction perpendicular to the plane of the flow. This component is familiarly interpreted as the stream function Ψ. An integral representation for Ψ is (Ref. 10):

$$\Psi(\vec{r},\,t) = \frac{1}{2}\int_R \omega(\vec{r}_o,\,t)\ln\frac{|\vec{r}|}{|\vec{r}_o-\vec{r}|}\,dR_o + \frac{1}{2\pi}\int_B\{(\vec{\nabla}_o\Psi(\vec{r}_o,\,t))\cdot\vec{n}_o - (\Psi(\vec{r}_o,\,t)\vec{n}_o\cdot\vec{\nabla}_o)\}\ln\frac{|\vec{r}|}{|\vec{r}_o-\vec{r}|}\,dB_o \tag{10}$$

The second integral in Eq. (10) again represents the contribution of the boundary condition. For a solid body translating in an infinite fluid, this contribution is simply $(\vec{v}_\infty\times\vec{r})\cdot\vec{k}$, where $\vec{k}$ is the unit vector in the direction perpendicular to the flow. Equation (10) becomes for this case

$$\Psi(\vec{r},\,t) = \frac{1}{2\pi}\int_{R_f}\omega(\vec{r}_o,\,t)\ln\frac{|\vec{r}|}{|\vec{r}_o-\vec{r}|}\,dR_o + (\vec{v}_\infty\times\vec{r})\cdot\vec{k} \tag{11}$$

Equations (10) and (11) are valid in the physical plane (x, y) and in any plane, say (ξ,η), related to the physical plane by a conformal transformation, with the stream function Ψ an invariant under the transformation. The vorticity in the (x,y)plane is related to that in the (ξ,η) plane by the following formula

$$\omega(\xi,\eta,\,t) = H^2\omega(x,\,y,\,t) \tag{12}$$

where H is the scale factor for the transformation and is defined by

$$H^2 = \left(\frac{\partial x}{\partial\xi}\right)^2+\left(\frac{\partial x}{\partial\eta}\right)^2 = \left(\frac{\partial y}{\partial\xi}\right)^2+\left(\frac{\partial y}{\partial\eta}\right)^2 \tag{13}$$

The position vector in the (x,y) plane is given by $\vec{r} = x\vec{i} + y\vec{j}$ and that in the (ξ,η) plane is given by $\vec{r} = \xi\vec{i} + \eta\vec{j}$.

Equation (11) or, equivalently, Eq. (9) forms the basis of earlier studies of the integro-differential approach by the present authors and by others. It has been pointed out (Ref. 8) that the operation count of numerical procedures based on these equations can be high. For example, suppose the vortical region of the flow contains N grid points. Equation (11) is represented by the algebraic equations

$$\Psi_i(t) = \sum_{j=1}^{N}\omega_j(t)F_{ji} + G_i,\quad i = 1,\,2,\,\ldots,\,N \tag{14}$$

where i refers to a grid point at which the value of Ψ is to be computed, j refers to a boundary point or a vortical point, F_{ji} are geometric coefficients whose values depend on the relative position of the points

i and j, and G_i are constant values corresponding to the last term of Eq. (11). The computation of each stream function value using Eq. (14) requires about 2N algebraic operations (N multiplicatons and N additions), provided that the geometric coefficients F_{ji} are known and need not be computed. The use of Eq. (14) to evaluate stream function values at all the N grid points requires a total of $2N^2$ algebraic operations. It is well known that an efficient finite-difference or finite-element solution of the two-dimensional form of Eq. (7) for a field containing N grid points requires a much smaller number of operations than $2N^2$. The use of the integral representation in the form of Eq. (11), or, equivalently, Eq. (9), is therefore computationally efficient only if the confinement of the solution field to the vortical regions results in a substantial reduction in the number of grid points required.

For many high Reynolds number flows, the vortical region constitutes only a small portion of the entire flowfield so that a substantial reduction in the needed number of grid points is indeed accomplished by the use of Eq. (11). It should be emphasized, however, that even if the reduction in the number of grid points is not substantial, the integro-differential approach still offers highly efficient numerical procedures.

One method of accomplishing superior computational efficiency is to use Eq. (11) only in the computation of stream function (or velocity) values at grid points surrounding the vortical regions. Once this is completed, the computation of stream function values at grid points in the vortical regions can be carried out using a finite-difference or a finite-element method. In this manner, the superiority of the integro-differential approach is assured since an optimum method, including a method that may appear in the future, can be incorporated into the numerical procedure and the solution field can be confined to the vortical regions.

Another method of improving the computational efficiency is to utilize a flowfield segmentation technique (Ref. 11). This technique has been suggested in conjunction with the velocity integrals, Eqs. (8), and (9) and tested on the problem of a flow past a finite flat plate. The application of this technique in conjunction with the stream function formulation is outlined here.

The flowfield is segmented into compartments each containing a suitable number of grid points. With known vorticity values at all grid points at a new time level, new stream function values at grid points located on the boundary of the compartments are computed from Eq. (14). Values of the normal gradient of the stream function at the compartment boundary are computed from an equation similar to Eq. (14) derived by differentiating Eq. (11) and representing the result by algebraic equations.

Stream function values at grid points located interior of the compartments are now computed using Eq. (10). Suppose the vortical region is segmented into several compartments each containing P number of grid points, with Q number of grid points located on the compartment boundary. Equation (10) is now represented for each compartment by the algebraic equations:

$$\Psi_i(t) = \sum_{j=1}^{P} \omega_j(t) F_{ji} + \sum_{j=1}^{Q} \left(\Psi_j M_{ji} + \frac{\partial \Psi}{\partial n}_j N_{ji} \right), \qquad i = 1, 2, \ldots P \tag{15}$$

where the first summation is over all grid points of the compartment and the second summation is over all grid points on the compartment boundary. The use of Eq. (15) to compute each stream function value requires 2(P+2Q) algebraic operations. This operation count is clearly substantially smaller than 2N if N is large. If the solution field is segmented into a larger number of compartments, then the operation count 2(P+2Q) decreases. On the other hand, with an increasing number of compartments, the total number of grid points located interior of all the compartments decreases. As a result, there are fewer grid points in the solution field for which the segmentation technique offers a computational advantage. At the same time, the number of grid points located on compartment boundaries increases with the number of compartments; and on these grid points not only the stream function value but also its normal gradient must be computed. There exists, therefore, an optimum number of compartments for each problem considered. This optimum number depends on the total number of grid points in the vortical region and the geometric distribution of these grid points. It is not difficult to show, however, that the optimum number of compartments in general increases with the total number of grid points. Consequently, the factor of reduction in the operation count also increases with the total number of grid points. For example, with 1089 grid points arranged in a 33 x 33 array, the operation count can be reduced by a factor of about 2.5 with the segmentation technique. With 4225 grid points arranged in a 65 x 65 array, the operation count can be reduced by a factor of about 4.6.

Substantial reductions in the total operation count for problems requiring a large number of grid points is a highly significant feature of the flowfield segmentation technique since it is precisely for these problems that excessive computer time presents a serious obstacle. An additional highly significant feature of this technique is the inherent flexibility it offers. The compartments utilized in the solution procedure can be of any arbitrary size or shape. Once the stream function (or velocity) values are established on the boundary of a compartment, the computation within that compartment can be performed independently of that in other compartments. Consequently, the flowfield segmentation technique is well suited for parallel programming.

Since the compartments can be chosen to be of standard simple shapes, such as rectangles, except near solid boundaries of irregular shape, various efficient methods can be adopted for the interior point computation. That is, one does not always need to use Eq. (15) for the interior point computation. Rather, highly efficient methods such as the fast Fourier transform method that are particularly well suited for simple boundary geometries can be utilized. If Eq. (15) is used, then the number of geometric coefficients that enters the computation procedure is drastically reduced by the use of compartments of standard shapes. Note that with Eq. (14), the number of geometric coefficients entering the computation is N^2. These geometric coefficients are independent of time. However, if N is very large, then the storage of the N^2 coefficients may present a problem, and the coefficients may need to be computed repeatedly for different time levels. With Eq. (15) and standard shape for compartments, the number of geometric coefficients is

P(P+2Q). This number can be further reduced to P+2Q if the compartments are rectangles and uniformly spaced grid is used in each compartment. These numbers are generally small enough so that all geometric coefficients can be stored.

As discussed earlier, the length scales for the potential and vortical regions of the flow are generally vastly different in magnitude. The use of the integral representation for the kinematic aspect of the problem makes it possible to confine the solid field to the vortical regions only. However, in the general viscous flow, the length scale within the vortical regions varies greatly. In the boundary-layers, the length scale is represented by the boundary layer thickness in the direction perpendicular to the solid surface. In the wake and recirculating regions, the length scale is represented by the body dimensions. The segmentation technique offers a convenient means of separating these parts of vortical regions in the solution procedure.

The above features of the segmentation technique are expected to be highly important for three-dimensional flows requiring the use of very large number of grid points. For the present studies of two-dimensional flows, only a few of these features of flowfield segmentation are incorporated into the solution procedure. It is noteworthy that the segmentation technique is useful also in the solution of the kinetic aspect of the problem. In the present study of the impulsively started airfoil problem, the solution field is divided into compartments in the kinetic part as well as the kinematic part of the computation.

3.4. Extraneous Vorticity Boundary Condition

The solution of Eq. (4) requires a knowledge of the vorticity values on the boundaries of the fluid as a function of time. The establishment of new vorticity values on solid boundaries is a necessary part of the overall solution procedure. In most of the previous investigations, one-sided difference formulas have been used to estimate the vorticity values on solid boundaries from the no-slip condition and the computed stream function (or velocity) values at grid points near the boundary. The computer time required for such calculations is very small compared to that required for the calculation of field values of vorticity. It has been found, however, that one-sided difference formulas of first-order accuracy tend to yield stable solutions, while second-order accurate formulas tend to give unstable results at high Reynolds numbers. In fact, for some problems, second-order formulas, even when stable, gave less accurate solutions than did the first-order formulas (Reference 19). The use of first-order formulas, however, restricts the overall accuracy of the solution. In particular, it has been shown (Reference 8) that first-order formulas do not permit the effect of tangential pressure gradient on the local boundary vorticity generation to be accounted for. There existed, therefore, considerable uncertainties regarding the correct one-sided formula to use, and regarding the limitations of each formula. These difficulties are independent of the computer time needed for the component problem under consideration, and are discussed more fully in Reference 8. They are referred to as the extraneous boundary-condition problem since the proper boundary condition for the physical problem is that for the velocity (or the stream function). The specification of the vorticity on the boundary of the fluid domain overspecifies the problem. These difficulties of extraneous boundary conditions, however, are not peculiar to the formulation of the problem using the vorticity as a field variable. If Eq. (1) is to be solved numerically instead of Eq. (4), then it is necessary to know the pressure on the solid boundaries in addition to the velocity.

The extraneous boundary-condition problem is absent in the boundary layer problem since the pressure in a direction normal to the boundary (vortical) layer is practically constant. Thus the pressure on the solid boundaries is equal to that at the outer edge of the boundary layer where it is determined by the outer flow. For the general viscous flow, the vortical region is not necessarily thin and the above simplification may not be valid.

In Ref. 8, it is shown that the prescribed velocity boundary condition imposes a kinematic restriction on the boundary vorticity values. The integral representation for the velocity vector then permits an accurate determination of the boundary vorticity value through the solution of an integral equation.

Consider, for example, a solid undergoing translation only. The second integral in Eq. (9) vanishes. If the vorticity distribution is known interior of the fluid domain R_f', then the first integral in Eq. (9) can be written as a sum of an integral over R_f' and an integral over the solid boundary B_s on which a layer of vorticity ζ exists. For two-dimensional flow, one then has, since $\vec{v} = 0$ in the solid,

$$\int_{B_s} \frac{\zeta_o (\vec{r}_o - \vec{r}_o^-)_n}{|\vec{r}_o - \vec{r}_o^-|^2} \, dB_o = F_b \tag{16}$$

where $\vec{r}_o^-$ is a point interior of the solid, n indicates a normal component, F_b is the tangential component of $\vec{F}$, which is defined by

$$\vec{F} = \int_{R_f'} \frac{\vec{\omega}_o \times (\vec{r}_o - \vec{r}_o^-)}{|\vec{r}_o - \vec{r}_o^-|^2} \, dR_o - 2\pi \vec{v}_\infty \tag{17}$$

With $\vec{\omega}$ known in R_f', $\vec{F}$ is determinate. Equation (16) therefore is a Fredholm integral equation containing ζ as the unknown function. This function ζ is rendered unique by the principle of conservation of total vorticity (Ref. 8) which requires

$$\int_{B_s} \zeta \, dB + \int_{R_f'} \omega \, dR = 0 \tag{18}$$

In previous studies, the integral equation (17) is approximated by a set of simultaneous algebraic equations containing ζ values at boundary grid points as unknown. The set of equations is solved using

iterative methods. In the present study, closed form solutions of the integral equation (17), subject to the restriction (18), are obtained. These closed form solutions make it possible to evaluate values on the solid boundaries explicitly, point by point. It is found that these explicit calculations yield highly accurate values of vorticity on solid boundaries. The derivations of the closed form solutions are presented in Ref. 1 and will also appear in future articles.

4. IMPULSIVELY STARTED AIRFOIL

The integro-differential formulation in terms of the stream function and vorticity is particularized, transformed, and applied to the study of the time-dependent incompressible viscous flow past an impulsively started 9% thick symmetric Joukowski airfoil at an angle of attack of 15^{o} and a Reynolds number of 1000. This problem has been studied previously by Mehta (Ref. 22) who mapped the fluid domain into the interior of a unit circle and used a finite-difference method to solve the transformed vorticity transport and Poisson's equations. In the present study, the geometry of the airfoil is identical to the one studied by Mehta. The vorticity transport equation and the integral representation are re-expressed in Mehta's transformed plane and Mehta's grid spacings are adopted in order to facilitate a comparison between the integro-differential results of the present study and the finite-difference results of Mehta.

The major features of the numerical procedures used in this study is described below for the component problems shown in Fig. 1.

The grid system is obtained through a transformation. This system is boundary-fitted and expanding. The shape of the 9% symmetric Joukowski airfoil is given in Figure 2 in the complex plane $z = x + iy$. By using the conformal transformation

$$z = \frac{1}{\kappa} + \gamma + \frac{\kappa C^2}{1 + \kappa} \tag{19}$$

where $\kappa = re^{i\theta}$, C and γ are real constants, the airfoil surface transforms into a circle and the exterior of the airfoil, i.e., the fluid domain, is mapped in the κ plane as the interior of the circle.

For the present problem, the values of C and γ are taken to be 0.9241635 and -0.05214 respectively. The coordinates and the flow variables are to be non-dimensionalized with respect to the radius of the circle and the freestream velocity. The non-dimensional chord length, L, of the airfoil is, according to equation (19), 3.71281277. The airfoil is 8.9998% thick.

The kinematic part of the computation is performed in the κ plane. A non-conformal transformation is utilized to obtain an efficient distribution of grid points for the kinetic part of the computation. The coordinate in the κ plane is not modified. The r coordinate is "stretched" by the relation (Ref. 22)

$$\rho = \frac{1}{4.8} \tanh^{-1}(1.996590918r - 1.032563339) + 2.8 \tag{20}$$

This transformation maps the annular region between $r = 0.02$ and $r = 1$ in the κ-plane into the interior of a unit circle in the ρ-θ plane.

The grid system in the $\rho - \theta$ plane is formed by using $\Delta\rho = 1/47$ and $\Delta\theta = \pi/40$. The coordinates of the grid point i,j are

$$\rho = 1.0 - (j - 1)\Delta\rho \quad \text{and} \quad \theta = (i - 1)\Delta\theta$$

Note that $j = 1$ corresponds to the airfoil surface and $j = 48$ ($\rho = 0$) corresponds roughly to a circle of radius 13 L in the physical plane. The corresponding grid system is shown in Fig. 2.

The vorticity distribution immediately after the start of the airfoil motion consists only of a vortex sheet on the airfoil. The determination of the initial vorticity distribution does not require a special procedure. Rather, the procedure outlined in Section 3.4. is applicable. With the vorticity everywhere zero in R_f', the vector $\vec{F}$, defined by Eq. (17), is simply $-2\pi v_\infty$. With this value of $\vec{F}$, Eq. (16) can be solved numerically to give the initial distribution of vorticity (vortex strength) on the airfoil surface. Alternatively, the closed form solution of Eq. (16), subject to the condition (18), is recognized to be

$$\zeta = 2v_\infty \sin(\theta + \alpha) \tag{21}$$

in the transformed plane. The corresponding vortex strength in the physical plane z is equal to ζ/H, H being the scale factor defined by

$$H = \left|\frac{dz}{d\kappa}\right| \tag{22}$$

The vorticity transport equation expressed in the working plane in terms of non-dimensional variables is

$$r^2 H^2 \frac{\partial\omega}{\partial t} = r\frac{d\rho}{dr}\left(\frac{\partial\Psi}{\partial\rho}\frac{\partial\omega}{\partial\theta} - \frac{\partial\Psi}{\partial\theta}\frac{\partial\omega}{\partial\rho}\right) + \frac{L}{Re}\left[\left(r\frac{d\rho}{dr}\right)^2\frac{\partial^2\omega}{\partial\rho^2} + r\left(\frac{d\rho}{dr} + r\frac{d^2\rho}{dr^2}\right)\frac{\partial\omega}{\partial\rho} + \frac{\partial^2\omega}{\partial\theta^2}\right] \tag{23}$$

where ω is the vorticity in the physical plane.

The vorticity transport equation (23) is approximated by an implicit finite-difference equation using a 3-point backward differencing to represent the time derivative:

$$\frac{\partial \omega}{\partial t} = \frac{1}{2\Delta t}\left(3\omega^{n+1} - 4\omega^{n} + \omega^{n-1}\right)$$

where the superscript refers to the time level. Space derivatives of vorticity are represented by central differencing at the time level n+1. The finite difference equation is of the form

$$B_{i,j}\,\omega^{n+1}_{i,j-1} + D_{i,j}\,\omega^{n+1}_{i-1,j} + E_{i,j}\,\omega^{n+1}_{i,j} + F_{i,j}\,\omega^{n+1}_{i+1,j}$$

$$+ H_{i,j}\,\omega^{n+1}_{i,j+1} = J_{i,j}\left(-2\omega^{n}_{i,j} + \frac{1}{2}\omega^{n-1}_{i,j}\right) \qquad (24)$$

The coefficients B, D, F and H contain derivatives of Ψ and are time-dependent. In the present work, the coefficients are evaluated at the time level n.

The selection of central differencing for the space derivatives of vorticity was made after comparing computed results for the first few time steps using central differencing with those using upwind differencing and using Arakawa differencing (Ref. 23). No significant deviations between the numerical values of vorticity was revealed. Mehta (Ref. 22) used Arakawa differencing, which requires more arithmetical operations than central differencing, to ensure total vorticity conservation. Since the present method of determining surface vorticity distribution conserves the total vorticity, the use of central differencing requiring fewer arithmetic operations is appropriate. Small amounts of spurious values of vorticity was found to occur in portions of the outer field where the vorticity values are expected to be negligible. Such occurences are perhaps attributable (Ref. 24, 25) to the large grid spacing, and hence cell Reynolds numbers, used in the present study in regions of the flow far from the airfoil surface. The use of upwind differencing in place of central differencing removes this anomalous solution behavior. Arakawa differencing was not found to be effective in removing this spurious vorticity. Since spurious vorticity values are very small and since they do not seriously affect the solution, it was decided to use central differencing which is higher ordered than upwind differencing.

A modified strongly implicit procedure (SIP) (Ref. 26) was used to solve the set of simultaneous algebraic equations (24) for vorticity values at the time level n+1. This method is selected amongst several competing methods on the basis of its solution efficiency and accuracy. The relative requirements of computer time using the various methods were, for the first few time steps, (a) Modified SIP - 100%, (b) SIP - 220%, (c) Alternating Direction Implicit (ADI) method - 154%, (d) Successive Line Relaxation - 254%, and (e) Successive Point Relaxation Method (used in Reference 22) - 365%. The ADI method is faster than the SIP method; but did not yield acceptable solution using the same time step sizes employed by the SIP method.

The SIP method was proposed by Stone (Ref. 26). Lin et al. employed the method successfully to obtain solutions for viscous flows past a cylinder. The basic concepts of this method as applied to the present problem is as follows. The coefficient matrix for Eq. (24) is sparse and contain only five non-zero diagonals. With a direct elimination procedure, one would factorize the coefficient matrix into the product of a lower and an upper triangular matrix, or use a procedure that is essentially equivalent. In such cases the triangular matrices generated are not in general sparse. With the SIP, the coefficient matrix is altered in such a manner that the altered matrix is easily factored into a product of a lower and an upper triangular matrix and that the matrices each have only three non-zero elements in each row.

With the SIP method, the solution field is bounded by the solid surface ($\rho = 1$) and a constant ρ line, say $\rho = \rho_1$ which is sufficiently removed from the non-negligible vorticity region. The value of ρ_1 is generally determined by the extent of the wake region. At large time levels, the wake extends far behind the airfoil while the vortical regions to the sides and ahead of the airfoil extend only a relatively short distance from the airfoil. As a result, a large number of data points where vorticity values are negligible enter into the solution procedure. The modification of the SIP method introduced in the present study consists of a division of the solution field into several compartments along constant θ lines, the individual application of SIP method in each compartment, and the use of successive line relaxation method for obtaining vorticity values along the dividing constant θ lines. With the solution field divided in this manner, each solution block is bounded by two constant θ lines, a part of the $\rho = 1$ line, and $\rho = \rho_1$ lines. ρ_1 can be different for different blocks. Therefore much fewer data points at which vorticity values are negligible enter into the computation. In the present study, the solution field is divided into four compartments. The location of the constant θ dividing lines and ρ_1 values are kept flexible and are changed in accordance with the shape of the non-negligible vorticity region as time progresses.

The vortex strengths on the airfoil surface are computed using an explicit formula in the transformed plane:

$$\xi = \frac{1}{2\pi}\int_{R_f'} \frac{\omega_o\left(r_o^2 - 1\right)_o dR_o}{1 + r_o^2 - 2r_o \cos\left(\theta_o - \theta\right)} + 2V_\infty \sin(\alpha + \theta) \qquad (25)$$

The value of the airfoil-boundary vorticity in the physical plane at a grid point located on the airfoil boundary is then obtained by dividing ξ by the scale factor H and by the physical distance corresponding to $\frac{1}{2}\Delta\rho$ nearest the airfoil surface. The surface vorticity values are re-calculated for each iteration. New boundary vorticity values for the subsequent iteration are obtained using a relaxation procedure and used in the SIP procedure for the calculation of vorticity values at grid points away from the boundary.

The computation of the stream function is accomplished using the flowfield segmentation technique described in Section 3.3. The flowfield is divided into several compartments. The boundary of the compartments are the $\theta = 0$ line and two ρ = constant lines. Stream function values on constant ρ compartment boundaries are computed using Eq. (14) in the transformed plane. Stream function values at the interior points of each compartment are then calculated using the strongly implicit method described earlier.

Instantaneous pressure distributions and shear stress on the airfoil surface are determined from the computed vorticity values and gradients on the surface in accordance with the following equations

$$\frac{\partial p}{\partial s} = \rho\nu \frac{\partial \omega}{\partial n} \tag{26}$$

and

$$\tau = \rho\nu\omega \tag{27}$$

Note that the direction of the normal coordinate is away from the fluid domain. Equation (26) is a specialization of Eq. (1) to the solid boundary S where the "no-slip" condition applies. The pressure and skin friction coefficients C_p and C_f are, from Eqs. (36) and (37), expressible as a function of θ as follows:

$$C_p(\theta) = \frac{2L}{Re} \frac{d\rho}{dr}\Big|_{\rho=1} \int_0^{\theta} \frac{\partial \omega}{\partial \rho}_{\rho=1} d\theta \tag{28}$$

and

$$C_f(\theta) = \frac{2}{Re} \omega\Big|_{\rho=1} \tag{29}$$

The force and moment are readily obtained from the computed values of $C_p(\theta)$ and $C_f(\theta)$, by numerical quadrature. In the present work, the values of $\partial\omega / \partial\rho$ are obtained by numerical differentiation using the values of $\omega_{i,1}$ and $\omega_{i,2}$.

Numerical results obtained for the airfoil problem are presented in Figs. 4 to 9. The chordwise distances from the leading edge, x_c and the load coefficients C_L, C_D, and C_M shown in the figures are normalized with respect to the chord length. The Reynolds number of 1000 is based on the chord length and the freestream velocity. All other quantities shown were normalized with respect to the freestream velocity and the radius of the unit circle. The reference time is the radius of the circle divided by the freestream velocity.

A check on the program coding was carried out by obtaining the solution for a flow past a circular cylinder at a Reynolds number of 40. The solutions were carried out up to a dimensionless time level of $t = 9.5$, the reference time being the cylinder radius divided by the freestream velocity. The drag coefficient at this time level is found to be 1.67 which is in reasonable agreement with an experimental value of 1.5 for steady state flow. The computed pressure distribution on the cylinder is compared with the experimental values (Ref. 28) in Figure 3.

Additionally, for the airfoil problem, the acceptibility of block subdivision was checked out by comparing the numerical results for a few first time steps of the following cases: (1) Successive Point and Line Relaxation Procedures without block subdivisions (2) Strongly Implicit Procedure (SIP) with no flow field subdivision (3) SIP method with four block subdivisions and for three different locations of block boundaries for the block enclosing the trailing edge. The excellent agreement of computed vorticity values for all these cases indicated the acceptability of block subdivision technique. The major aspects of the flow phenomena past the impulsively started airfoil at an angle of attack of 15° and at a Reynolds number of 1000 are described below.

At time $t = 0$, the flow around the airfoil corresponds to that of a non-circulatory potential flow. After the impulsive start the rear stagnation point (RSP) moves very rapidly to the trailing edge (TE) from its potential flow location of $X_c = 0.9808$. This rapid movement of the rear stagnation point is accompanied by a small separation bubble located between RSP and TE at time levels 0.003 and 0.004. After the RSP has reached the TE, plots of equi-vorticity contours show "curling up" of vorticity field near trailing edge with positive vorticity values in the curled up regions. The curling up of vorticity field is indicative of vortex roll-up and the formation of starting vortex. The vorticity in this starting vortex diffuses rapidly.

An adverse pressure gradient on the upper surface becomes noticeable at time $t = 0.068$. At time $t = 0.404$ this adverse pressure gradient is more pronounced (Fig. 4) and this leads to the birth and growth of the first separation bubble with clockwise flow. This bubble eventually extends over almost the entire upper surface of the airfoil, at time $t = 6.228$ (Fig. 5a). At the very next time level, $t = 6.74$, its re-attachment point separates from the airfoil. In Figure 5, streamlines are shown around the airfoil for several time levels. The values of the stream function are in the range -0.48 to 0.48 in steps of 0.04. As the bubble size increases the pressure gradient on the upper surface decreases as seen from Fig. 4. The lift coefficient which has been rapidly decreasing after the impulsive start (Fig. 6), begins to increase with the growth of the clockwise bubble A, as seen from Fig. 7. This increase in lift is associated with the fact that the attached bubble effectively increases the camber of the airfoil. After the bursting of the bubble at time $t = 6.74$, the lift coefficient increases at much slower rate and it starts falling off at time $t = 9.0$ (Fig. 8). The bursting of the bubble causes the drag coefficient to increase (Fig. 8), since the wake width is increased for the separated flow.

An adverse pressure gradient for the reversed flow on the upper surface from X_c 0.82 to X_c 0.6 is noticeable in Fig. 9. A counterclockwise bubble, B, appears in this region and grows with time. The growth of this counterclockwise bubble causes the lift coefficient to fall off rapidly (Fig. 8). From time $t = 6.74$ to $t = 17.62$ there is no rear stagnation streamline and the rear stagnation point becomes the separation point of a counterclockwise bubble, C (Fig. 5b). The growth of bubble B partitions the recirculating region

A into regions A' and D (Fig. 5b). Also bubbles B and C merge together and then lift off from the surface at time t = 17.748 (Fig. 5c). At this time level region D becomes an attached clockwise bubble, and subsequently at time t = 18.26 a counterclockwise bubble, E, appears within the attached bubble D. Growth of this counterclockwise bubble E divides bubble D into two parts (Fig. 5d). As time progresses, bubble D' of Fig. 5d moves towards the trailing edge and bursts. After the bursting of D', the bubble D grows rapidly in size and at time t = 25.428 it extends over almost the entire upper surface of the airfoil.

The present results are in good agreement with those of Mehta (Ref. 22) until the bursting of the first separation bubble. After this the sequence of occurence of bubbles and their bursting or lift off from surface are different between these two studies. The key differences are the following: (1) In the present study, whenever there is no rear stagnation streamline, a small counterclockwise trailing edge bubble is always present and the rear stagnation point becomes the separation point of this bubble. This is not found true in Mehta's study. (2) After bubbles B and C merge they stay merged and lift off from the surface together. In Mehta's study they separate again and only bubble C lifts off to surface. Bubble B stays on the surface to play the roll of bubble E of the present case.

The following general conclusions are similar between the two studies. (1) Immediately after impulsive start the rear stagnation point moves very rapidly to the trailing edge. (2) Subsequently a "starting vortex" is visualized through concentric equivorticity lines. (3) The formation of a separation bubble is preceded by an adverse pressure gradient (4) Clockwise bubbles extend or move towards trailing edge and burst (5) Anticlockwise bubbles either lift off the surface or open up to streamlines from above the surface (6) The lift increases with increase in the size of attached clockwise bubbles and decreases when attached anticlockwise bubbles grow.

5. OSCILLATING AIRFOIL

The integro-differential formulation in terms of the velocity vector and the vorticity is utilized in the study of incompressible flows past a 12% thick symmetric Joukowski airfoil oscillating in pitch about a pitching axis located 1/4 chord from the leading edge. The major features of the numerical procedures are described below in terms of the component problems shown in Fig. 1.

The solution field, already confined to the vortical region, is divided into an inner region and an outer region. In the inner region, the grid system consists of grid points, or nodes, that are not uniformly spaced. The nodes represent vortices of triangular elements. In Fig. 10 is shown the specific grid system for the inner region used with the 12% thick airfoil. This system has 232 nodes, including 48 nodes on the airfoil surface and 62 nodes on the outer boundary of the inner region. This system gives 354 triangular elements. The grid system for the outer region consists of uniformly spaced grid points forming a rectangular array. The outer region overlaps the inner region by one layer of elements. That is, in the outermost layer of triangular elements, each pair of elements form a rectangle whose boundaries coincide with the rectangular grid lines of the outer region. The grid spacings used for the airfoil are $\Delta x = 0.05$ and $\Delta y = 0.025$. This grid system for the outer region is not shown in Fig. 10. The number of grid points in the outer region is large. In the oscillating airfoil case, more than 3500 points are used in the outer region.

A finite-element method is used to treat the kinetics of the problem in the inner region. In the outer region, finite-difference methods are used. This hybrid finite element-finite difference method permits the grid system to "fit" the airfoil boundary geometry and to have relatively closely spaced grid points near the airfoil boundary. By using a relatively small number of nodes in the inner region, the size of the relatively complex coefficient matrices involved in the finite-element method is kept small. Most of the solution field is covered by the finite-difference grid which leads to relatively simple coefficient matrices.

Associated with each node "i" in the inner region at (x, y), there is a composite linear interpolation function $N_i(x, y)$ with the property

$$N_i(x_j, y_j) = \zeta_{ij} \tag{30}$$

where ζ_{ij} is the Kronecker delta. The interpolation function is continuous across the element boundaries (It is zero in elements not containing the node i) though its first derivatives are not necessarily continuous. The velocity and the vorticity fields are assumed to vary linearly within each element. Thus one writes

$$\omega = \begin{pmatrix} N_i, & N_j, & N_k \end{pmatrix} \begin{Bmatrix} \omega_i \\ \omega_j \\ \omega_k \end{Bmatrix} \tag{31}$$

for the triangular element with nodes i, j and k. Using Galerkin's procedure, an approximation to the two-dimensional vorticity transport equation is

$$\int_R \left(\frac{\partial \omega}{\partial t} + u \frac{\partial \omega}{\partial x} + v \frac{\partial \omega}{\partial y} - \nu \nabla^2 \omega \right) N_i(x, y) dx dy = 0 \tag{32}$$

The above weighting process is applied at all nodes in the inner region except those on the boundary of that region. By the use of the divergence theorem, one obtains

$$\nu \int_R (\nabla^2 \omega) N_i dx\, dy = -\nu \int_R \vec{\nabla} N_i \cdot \vec{\nabla} \omega \, dx dy$$

$$+ \nu \int_B N_i (\vec{\nabla} \omega) \cdot \vec{n} dB \tag{33}$$

The line integral is performed over the boundary of the inner region. Since i is not a boundary node, this line integral vanishes by virtue of Eq. (30). By the use of Eq. (33), the integrand in Eq. (32) is re-expressed as one containing only first derivatives of ω.

Equation (32) can be written as the sum of component integrals over all elements in the inner region. Upon introducing Eq. (31) into the integrals, each of the component integrals in the sum can be integrated, yielding a system of simultaneous differential equations of the form

$$[H]\left\{\frac{d\omega}{dt}\right\} + [C]\{\omega\} + [D]\{\omega\} = \{E\} \tag{34}$$

Using a backward difference scheme for the time derivative, one obtains

$$[H]\left\{\frac{\omega^{n+1}-\omega^{n}}{\Delta t}\right\} + [C^{n}]\{\omega^{n+1}\} + [D]\{\omega^{n+1}\} = \{E^{n+1}\} \tag{35}$$

The terms on the left hand side of Eq. (32) represent respectively the local time rate of change of vorticity, the convection of vorticity, and the diffusion of vorticity. The coefficient matrices $[H]$ and $[D]$ are depdendent only on the node coordinates and are independent of time, they do not need to be evaluated repeatedly for different time levels. The matrix $[C]$ represents convective processes and is dependent on time through the time-varying velocity distribution. To avoid iterative computation of the velocity values for each time step, the velocity field is computed only for the old time step "n". The column matrix $\{E\}$ on the right hand side of Eq. (35) is also time dependent. It represents the contributions of the boundary nodes of the inner region. With known vorticity values on the boundary nodes, $\{E\}$ can be explicitly computed. In the present work, the boundary of the inner region consists of the solid surface and the boundary located within the outer region. (Recall that the two regions overlap). Vorticity values at boundary nodes that are located inside the outer region are computed as a part of the finite-difference procedure. Vorticity values at the solid surface are determined as a part of the kinematic computation as described in Section 3.4.

Since the matrix $[C]$ is time-dependent, the coefficient matrix of the system of simultaneous algebraic equations for the unknown ω^{n+1} must be inverted at each time step. It should be noted, however, that fairly large time intervals can be used in the solution procedure.

In the outer region, the vorticity transport equation is treated using a two-point backward time differencing scheme, with successive point overrelaxation method used to solve the resulting algebraic equations.

The velocity values are computed by a numerical quadrature of Eq. (9). The first integral in Eq. (9) is expressed as a sum of component integrals over individual elements. (For this purpose, each rectangle bounded by grid lines in the outer region is treated as a rectangular element). The use of interpolation functions then leads to exact analytical expressions for the component integrals. These exact expressions have been derived for interpolation functions of all degrees. In the present work, linear interpolation functions are used for the triangular elements of the inner region of the grid system. The vorticity in the rectangular elements of the outer region, however, are represented by a concentrated vortex filament placed at the centroid of the element and its contribution to the velocity field is computed in accordance with the Biot-Savart law. The evaluation of the second integral in Eq. (9) is simplified by considering the rotating coordinate system and the nonrotating coordinate system to coincide with one another at the time t. The second integral can then by re-expressed as

$$2\vec{\Omega}(t) \times \int_{R_s} \frac{\vec{r}_o - \vec{r}}{|\vec{r}_o - \vec{r}|^{d}}\, dR \tag{36}$$

The integral therefore needs to be evaluated only for unit angular velocity $\Omega = 1$ since it is directly proportional to Ω.

The computation of the pressure and skin friction coefficients are carried out in the manner described in Section (4).

The numerical procedures used in this study were calibrated by treating the problem of a flow past an impulsively started finite flat plate at a Reynolds number of 1000 and at zero angle of attack. The results obtained are in excellent agreement with earlier results (Ref. 8) obtained using finite-difference methods instead of the present hybrid method in treating the vorticity transport equation. The solution was carried to a dimensionless time level of 2.4, the reference time level being the plate length divided by the freestream velocity. At this time level, the solution varies very slowly with time in the vicinity of the plate. The velocity and vorticity profiles at midplate obtained for this large time level are, as expected, in excellent agreement with the Blasius profile.

As an additional calibration, the flow past an impulsively started circular cylinder at a Reynolds number based on the cylinder diameter of 40 was treated. The solution was carried to a dimensionless time level of 20.4. At this time level, the computed drag coefficient varies only in the fourth significant digit between successive time levels, the time step being 0.125. The computed streamline and constant vorticity contours are shown in Fig. 11, in the upper and lower halves of the figure respectively, for this large time level. The computed pressure distribution around the cylinder is shown in Figure 3, compared with the results described in Section 4 and experimental results (Ref. 28).

The case where the airfoil is set into translational motion impulsively at an angle of attack of 3° and a Reynolds number of 1000 was studied. The transient solution after the onset of the motion is carried to a dimensionless time level of 2.07, the reference time being the chord length divided by the freestream velocity. The streamline pattern at a time level of 0.87 is shown in Fig. 12. The adverse pressure gradient on the upper surface was not sufficiently strong to cause flow separation. The streamline pattern, however,

shows a thick boundary layer region on the upper surface.

The loads on the airfoil are very high immediately after the impulsive start. They decrease rapidly at small time levels, up to a dimensionless time level of 0.35. Prior to this time level, the loads are due primarily to the impulsive start effects. Subsequent to this time level, viscous effects, particularly the thickening of the boundary layer, results in further changes of the loads. The surface pressure decreases relative to the trailing edge pressure. The upper surface pressure, however, decreases at a more rapid rate so that the lift coefficient increases with time. Figure 13 shows the variation of the lift coefficient C_L and of the drag coefficient C_D over the time interval form 0.3 to 2.07. Both the lift and the drag coefficients vary relatively slowly at the time level 2.07.

A flow past the airfoil oscillating at a moderate reduced frequency of 0.3 and a Reynolds number of 1000 was treated. The airfoil is set into translational motion impulsively at $t = 0$. The angle of attack α is given by

$$\alpha = 3^{\circ} + 1^{\circ} \sin(0.6t) \tag{37}$$

The solution was carried to a non-dimensional time level of 10.4. The airfoil undergoes a complete cycle of oscillation during this period.

The main feature of the load history is that the lift and moment agree qualitatively with the time-dependent linearized potential flow solution. The calculated lift variation is in phase with the potential flow result. The magnitude of the lift coefficient is lower than the lift predicted by the potential flow analysis. This is expected since at the moderate Reynolds number of 1000, the boundary layer on the upper surface is thick and its displacement thickness results in a significant change in the effective shape of the airfoil.

The viscous drag is much larger than the pressure drag for the present case of low angle of attack. This viscous drag is relatively insensitive to the pitching motion of the airfoil. Numerical results indicate a very small separation bubble appearing near the trailing edge on the upper surface during the down stroke (not at maximum angle of attack). However, the size of this bubble is very small and the presence of the bubble does not affect the integrated load significantly.

The solution obtained at the end of the moderate-frequency oscillation cycle was used as the initial solution for a high frequency oscillation computation. The flow Reynolds number is 1000 and the reduced frequency is 3 for this case. The angle of attack is given by

$$\alpha = 3^{\circ} + 1^{\circ} \sin(6t) \tag{38}$$

The computation was performed for more than two cycles of oscillation. The transient effect, due to the initial condition used, is present during the first cycle but became very small during the second cycle. The load history is presented in Figures 14, 15, 16 and 17.

6. REFERENCES

1. Sampath, S., "A Numerical Study of Incompressible Viscous Flow Around Airfoils," Ph.D. Thesis, Georgia Institute of Technology, 1977.

2. Wu, J. C. and Thompson, J. F., "Numerical Solutions of Time-Dependent Incompressible Navier-Stokes Equations Using an Integro-Differential Formulation," Vol. 1, No. 2, pp. 197-215, Journal of Computers and Fluids, 1973.

3. Wu, J. C., and Sugavanam, A., "A Method for the Numerical Solution of Turbulent Flow Problems," AIAA Paper No. 77-649, Proceedings of AIAA 3rd Computational Fluid Dynamics Conference, 1977.

4. Wu, J. C., "Integral Representations of Field Variables for the Finite Element Solution of Viscous Flow Problems," Proceedings of the 1974 Conference on Finite Element Methods in Engineering, Clarendon Press, 1974.

5. Wu, J. C., "Finite Element Solution of Flow Problems Using Integral Representation," Proceedings of Second International Symposium on Finite Element Methods in Flow Problems, International Centre for Computer Aided Design, Conference Series No. 2/76, June 1976.

6. Wu, J. C., and Wahbah, M., "Numerical Solution of Viscous Flow Equations Using Integral Representations," Lecture Series in Physics, Springer-Verlag, Vol. 59, 1976.

7. Thompson, J. F., Shanks, S. P., and Wu, J. C., "Numerical Solution of Three-Dimensional Navier-Stokes Equations Showing Trailing Tip Vortices," AIAA Journal, Vol. 12, No. 6, pp. 787-794, June 1974.

8. Wu, J. C., "Numerical Boundary Conditions for Viscous Flow Problems," AIAA Journal, Vol. 14, No. 8, 1976.

9. Wu, J. C., and Sankar, N. L., "Explicit Finite Element Solution of the Viscous Flow Problem," Proceedings of the 1976 International Conference on Finite Element Methods in Engineering, 1976.

10. Wu, J. C., and Thompson, J. F., "Numerical Solution of Unsteady, Three-Dimensional Navier-Stokes Equations," Proceedings Project SQUID Workshop on Fluid Dynamics of Unsteady, Three-Dimensional, and Separated Flows, October, Purdue University, Lafayette, Indiana, October, 1971.

11. Wu, J. C., Spring, A. H. and Sankar, N. L., "A Flowfield Segmentation Method for the Numerical Solution of Viscous Flow Problems," Proceedings of the Fourth International Conference on Numerical Methods in Fluid Dynamics, Lecture Notes in Physics, Vol. 35, Springer-Verlag, 1975.

12. Schmall, R. A., and Kinney, R. B., "Numerical Study of Unsteady Viscous Flow Past a Lifting Plate," AIAA J., Vol. 12, No. 11, 1974.

13. Kinney, R. B., and Paolino, M. A., "Flow Transient Near the Leading Edge of a Semi-Infinite Flat Plate Moving Through a Viscous Fluid, J. Applied Mech., Vol. 41, No. 4, 1974.

14. Panniker, P. K. G. and Lavan, Z., "Flow Past Impulsively Started Bodies Using Green's Functions," J. Computational Phys., Vol. 18, No. 1, 1975.

15. Reddy, R. N., and Thompson, J. F., "Numerical Solution of Incompressible Navier-Stokes Equations in the Integro-Differential Formulation," AIAA Paper No. 77-650, Proceedings of AIAA 3rd Computational Fluid Dynamics Conference, 1977.

16. Davis, R. T., "Numerical Solution of the Incompressible Navier-Stokes Equations for Two Dimensional Flows at High Reynolds Number," Rept. No. AFL 76-8-22, Department of Aerospace Engineering, University of Cincinnati, 1976.

17. Thompson, J. F., Thames, F. C., and Mastin, C. W., "Automatic Numerical Generation of Body-Fitted Curvilinear Coordinate System for Field Containing Any Number of Arbitrary Two-Dimensional Bodies," J. Computational Phys., Vol. 15, No. 3, 1974.

18. "Proceedings of the Second International Symposium on Finite Element Methods in Flow Problems," International Centre for Computer Aided Design, Conference Series No. 2/76, 1976.

19. Roache, P. J., "Computational Fluid Dynamics," Hermosa Publishers, Albuquerque, New Mexico, 1972.

20. Cheng, S. I., "Numerical Integration of Navier-Stokes Equations," AIAA Journal, Vol. 8, No. 12, 1970.

21. Moretti, G., "Importance of Boundary Conditions in the Numerical Treatment of Hyperbolic Equations," Phys. Fluids, Vol. 12, No. 12, 1969.

22. Mehta, U. B., "Starting Vortex, Separation Bubbles and Stall -A Numerical Study of Laminar Unsteady Flow Around an Airfoil," Ph.D. Thesis, Illinois Inst. of Tech., Chicago, 1972.

23. Arakawa, A., "Numerical Solution of Large Scale Atmospheric Motions," SIAM-AMS Proceedings, Vol. 2, Numerical Solution of Field Problems in Continuum Physics, American Math. Soc., 1970.

24. Lugt, H. J., and Hausling, H. J., "Laminar Flow Past an Abruptly Accelerated Elliptic Cylinder at 45 degree Inclination," J. Fluid Mechanics, Vol. 65, Oct. 2, 1974, pp. 711-734.

25. Lin, C. L. and Lee, S. C., "Transient State Analysis of Separated Flow Around a Sphere," Computers and Fluids, Vol. 1, pp. 235-250, 1973.

26. Stone, H. L., "Iterative Solution of Implicit Approximations of Multi-dimensional Partial Differential Equations," SIAM J. Num. Analysis, Vol. 5, No. 3, pp. 530-558, 1969.

27. Lin, C. L., Pepper, D. W., and Lee, S. C., "Numerical Methods for Separated Flow Solution Around a Circular Cylinder," Proc. of AIAA 2nd Computational Fluid Dynamics Conference, Hartford, Connecticut, June 19-20, 1975, pp. 91-100.

28. Grove, A. S., Shair, F. H., Petersen, E. E., and Acrivos, A., "An Experimental Investigation of the Steady Separated Flow Past a Circular Cylinder," J. Fluid Mech., Vol. 33, Part 1, 1964, pp. 60 80.

7. ACKNOWLEDGEMENT

This paper is based on research supported by the Office of Naval Research under Contract No. N00014-75-C-0249.

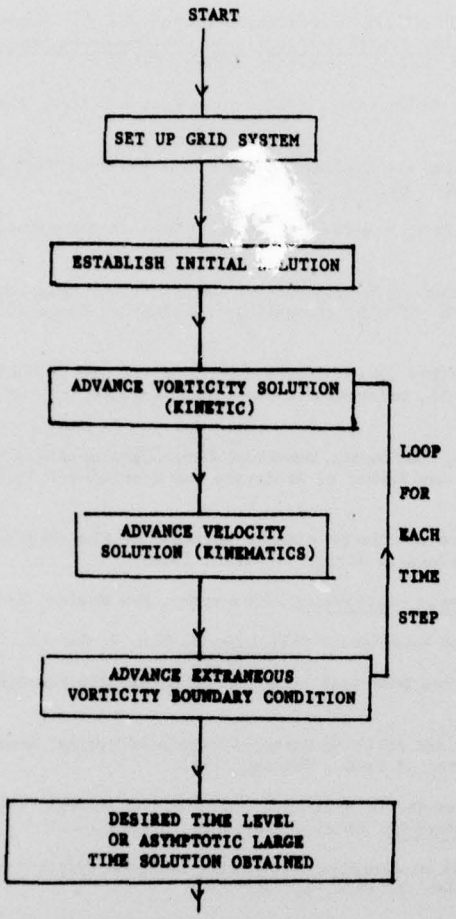

Fig. 1. COMPONENT PROBLEMS FOR THE GENERAL VISCOUS FLOW

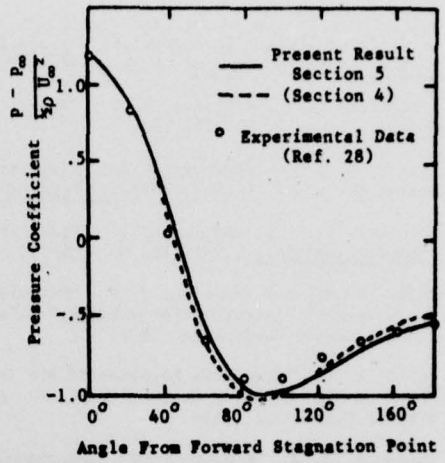

Fig. 3. PRESSURE DISTRIBUTION OVER A CIRCULAR CYLINDER ($U_\infty D/\nu = 40$)

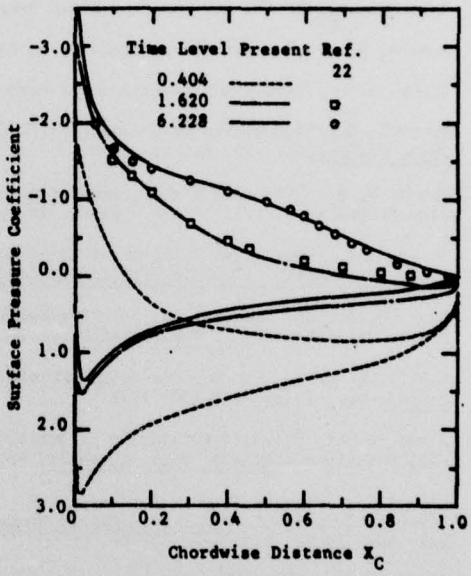

Fig. 4. SURFACE PRESSURE DISTRIBUTION OVER A 9% JOUKOWSKI AIRFOIL AT 15° ANGLE OF ATTACK FOR EARLY TIME LEVELS

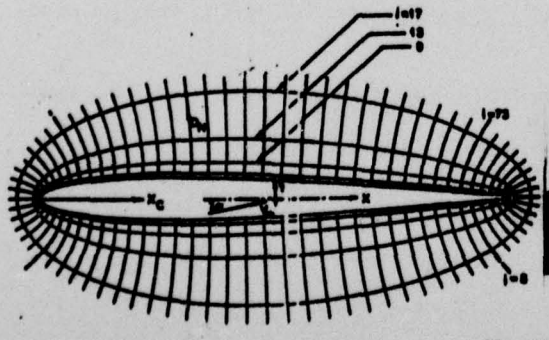

Fig. 2 GRID DISTRIBUTION AND NOTATIONS IN PHYSICAL PLANE

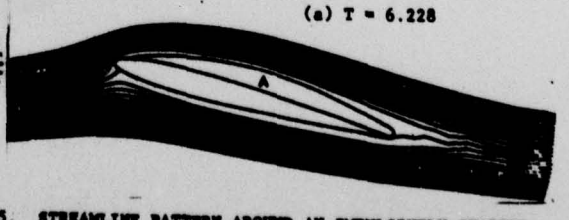

Fig. 5. STREAMLINE PATTERN AROUND AN IMPULSIVELY STARTED 9% JOUKOWSKI AIRFOIL AT 15° ANGLE OF ATTACK AT SELECTED TIME LEVELS

(b) T = 16.084

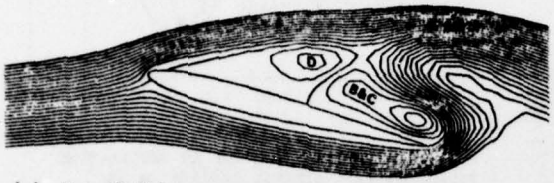

(c) T = 17.748

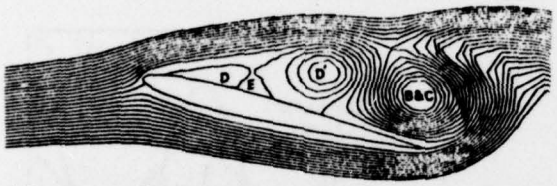

(d) T = 19.284

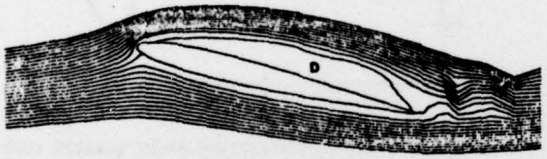

(e) T = 25.428

Fig. 5 Continued

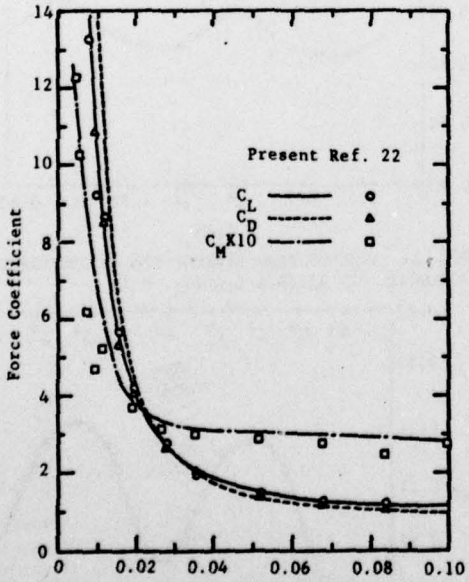

Fig. 6. LOAD HISTORIES FOR AN IMPULSIVELY STARTED JOUKOWSKI 9% AIRFOIL AT 15° ANGLE OF ATTACK AT EARLY TIME LEVELS

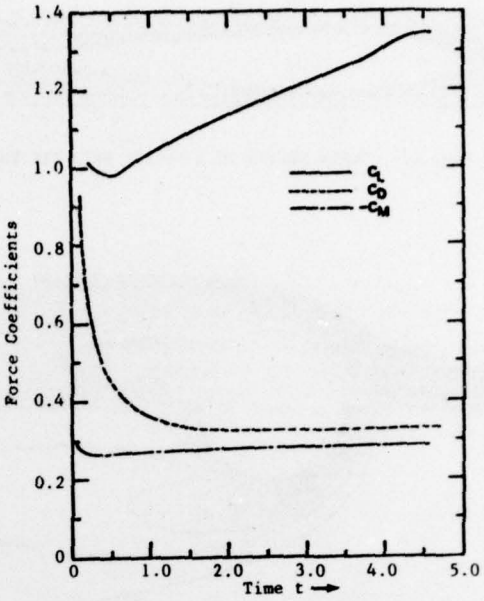

Fig. 7. LOAD HISTORIES FOR AN IMPULSIVELY STARTED 9% JOUKOWSKI AIRFOIL AT 15° ANGLE OF ATTACK

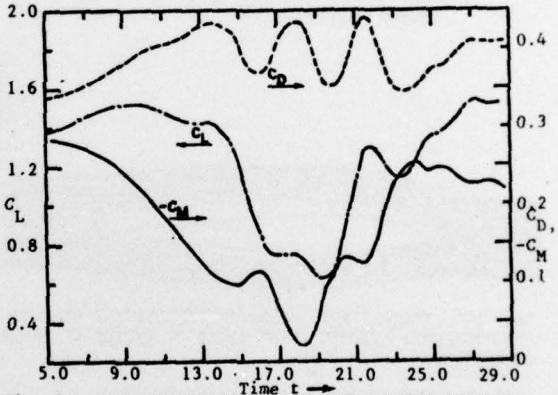

Fig. 8. LOAD HISTORIES FOR AN IMPULSIVELY STARTED 9% JOUKOWSKI AIRFOIL AT 15° ANGLE OF ATTACK

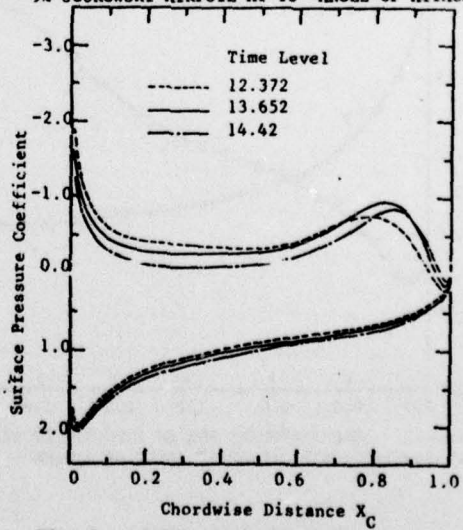

Fig. 9. SURFACE PRESSURE DISTRIBUTION OVER AN IMPULSIVELY STARTED 9% JOUKOWSKI AIRFOIL AT 15° ANGLE OF ATTACK

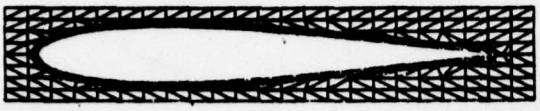

Fig. 10. INNER REGION OF A HYBRID GRID SYSTEM

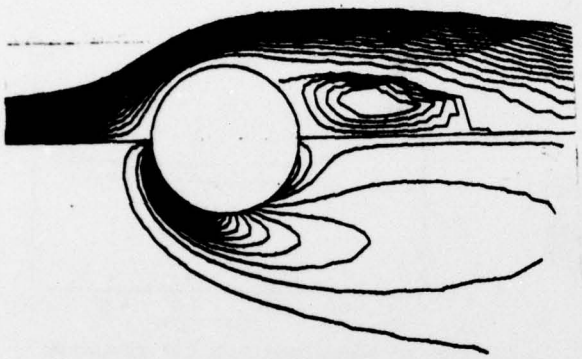

Fig. 11. STREAMLINES AND VORTICITY CONTOURS FOR VISCOUS FLOW OVER A CIRCULAR CYLINDER AT LATER TIME LEVELS ($U_\infty D/\nu$ = 40)

Fig. 12. STREAMLINES AROUND AN IMPULSIVELY STARTED 12% JOUKOWSKI AIRFOIL AT 3° ANGLE OF ATTACK AT EARLY TIME LEVELS

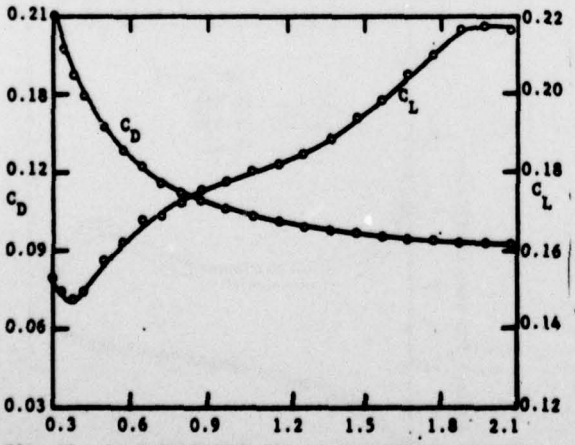

Fig. 13. LOAD HISTORIES FOR AN IMPULSIVELY STARTED 12% JOUKOWSKI AIRFOIL AT 3° ANGLE OF ATTACK

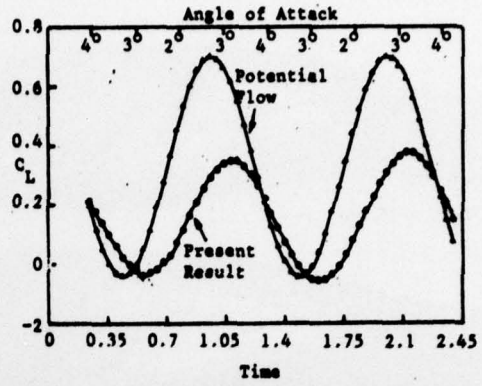

Fig. 14. LIFT HISTORY FOR AN OSCILLATING JOUKOWSKI 12% AIRFOIL ($\omega C/2\,U_\infty$ = 3)

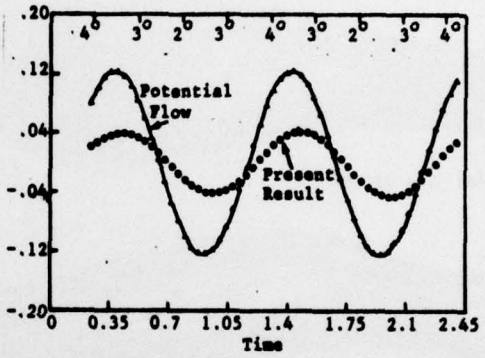

Fig. 15. MOMENT COEFFICIENT ABOUT QUARTER CHORD FOR AN OSCILLATING JOUKOWSKI 12% AIRFOIL ($\omega C/2U_\infty$ = 3)

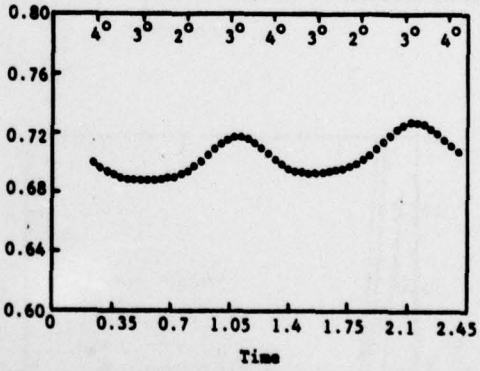

Fig. 16. VISCOUS DRAG HISTORY FOR AN OSCILLATING JOUKOWSKI 12% AIRFOIL ($\omega C/2U_\infty$ = 3)

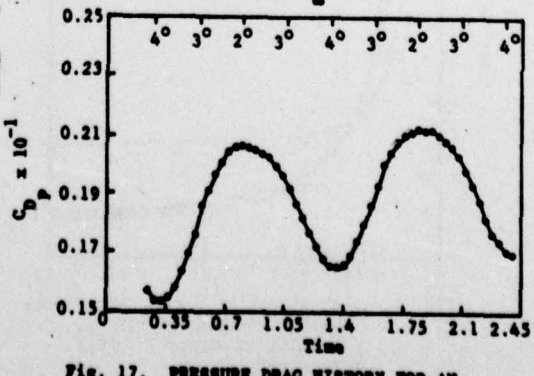

Fig. 17. PRESSURE DRAG HISTORY FOR AN OSCILLATING JOUKOWSKI 12% AIRFOIL ($\omega C/2U_\infty$ = 3)